

Wild-type and mutant SOD1 share an aberrant conformation and a common pathogenic pathway in ALS

Daryl A Bosco^{1,8}, Gerardo Morfini^{2,7,8}, N Murat Karabacak³, Yuyu Song^{2,7}, Francois Gros-Louis⁴, Piera Pasinelli⁵, Holly Goolsby⁶, Benjamin A Fontaine¹, Nathan Lemay¹, Diane McKenna-Yasek¹, Matthew P Frosch⁶, Jeffrey N Agar³, Jean-Pierre Julien⁴, Scott T Brady^{2,7} & Robert H Brown Jr¹

Many mutations confer one or more toxic function(s) on copper/zinc superoxide dismutase 1 (SOD1) that impair motor neuron viability and cause familial amyotrophic lateral sclerosis (FALS). Using a conformation-specific antibody that detects misfolded SOD1 (C4F6), we found that oxidized wild-type SOD1 and mutant SOD1 share a conformational epitope that is not present in normal wild-type SOD1. In a subset of human sporadic ALS (SALS) cases, motor neurons in the lumbosacral spinal cord were markedly C4F6 immunoreactive, indicating that an aberrant wild-type SOD1 species was present. Recombinant, oxidized wild-type SOD1 and wild-type SOD1 immunopurified from SALS tissues inhibited kinesin-based fast axonal transport in a manner similar to that of FALS-linked mutant SOD1. Our findings suggest that wild-type SOD1 can be pathogenic in SALS and identify an SOD1-dependent pathogenic mechanism common to FALS and SALS.

ALS is an adult-onset, motor neuron disease that causes progressive degeneration of motor neurons and death within 3–5 years of diagnosis¹. The most prevalent factors associated with inherited forms of ALS (FALS) are mutations in the *SOD1* gene, which encodes cytosolic Cu/Zn superoxide dismutase². In FALS, cytotoxicity of motor neurons appears to result from a gain of toxic SOD1 function, rather than from a loss of dismutase activity³. Although the exact molecular mechanisms underlying mutant SOD1-mediated motor neuron degeneration are unclear, prevailing hypotheses suggest that mutation-induced conformational changes lead to SOD1 misfolding and subsequent aggregation^{4–9}.

The etiology of SALS, which accounts for ~90% of ALS, is largely unknown. In contrast, several genetic variants have been identified in association with FALS². That FALS and SALS are clinically and neuropathologically similar implies that the pathogenesis of these diseases must converge on a common pathogenic pathway and/or involve similar toxic factors, but such factors have remained elusive^{1,10}. Wild-type SOD1 has been proposed as a potential link between SALS and FALS^{11,12}, although the existence of a toxic wild-type SOD1 species that is associated with SALS *in vivo* and that recapitulates the pathogenic features of mutant SOD1 has not been demonstrated. One hypothesis states that defects in the normal post-translational modifications of wild-type SOD1 or the introduction of aberrant covalent modifications to wild-type SOD1 could induce conformational

changes in wild-type SOD1 that mimic structural features of FALS SOD1 mutants^{13–15}. Several lines of evidence support this view, including reports that metal-depleted^{16,17} and oxidized^{11,18} wild-type SOD1 increasingly misfold *in vitro*¹⁹ and are toxic when exogenously administered to cells^{11,17}. These observations suggest that aberrantly modified wild-type SOD1 and FALS-linked SOD1 mutants share similar structural features; however, common pathogenic mechanisms triggered by FALS- and SALS-related SOD1 species remain elusive.

Recently, a monoclonal antibody (C4F6) was generated against the FALS-linked SOD1 G93A mutant protein and was shown to preferentially bind to several FALS-linked SOD1 mutant proteins rather than to wild-type SOD1 (ref. 20). Thus, C4F6 appears to be specific for a particular conformation inherent in misfolded SOD1. If aberrant modifications to wild-type SOD1 induce the protein to adopt a mutant-like conformation, we speculated that the C4F6 antibody could detect misfolded wild-type SOD1 species associated with SALS. Moreover, if wild-type SOD1 has a pathogenic role in SALS, we would expect these aberrant wild-type SOD1 species to recapitulate one or more toxic effect(s) of FALS-linked SOD1 mutants. We examined SALS-associated wild-type SOD1 species using the C4F6 antibody *in vitro* and *in vivo*. Our recent finding that FALS-linked, mutant SOD1 protein inhibits fast axonal transport (FAT) (G.M. and S.T.B., unpublished observations, and ref. 10) led us to investigate potential toxic properties of wild-type SOD1 that had undergone misfolding

¹Department of Neurology, University of Massachusetts Medical Center, Worcester, Massachusetts, USA. ²Department of Anatomy and Cell Biology, University of Illinois at Chicago, Chicago, Illinois, USA. ³Department of Chemistry, Brandeis University, Waltham, Massachusetts, USA. ⁴Department of Psychiatry and Neuroscience, Laval University, Research Centre of CHUQ, Quebec, Canada. ⁵Weinberg Unit for ALS Research, Farber Institute for the Neurosciences, Thomas Jefferson University, Philadelphia, Pennsylvania, USA. ⁶C.S. Kubik Laboratory for Neuropathology, Massachusetts General Hospital, Boston, Massachusetts, USA. ⁷Marine Biological Laboratory, Woods Hole, Massachusetts, USA. ⁸These authors contributed equally to this work. Correspondence should be addressed to D.A.B. (daryl.bosco@umassmed.edu) or R.H.B. Jr (robert.brown@umassmed.edu).

in association with SALS using the same experimental model²¹. We found that the SOD1 protein can become pathogenic via nonhereditary modifications (for example, oxidation), thus supporting the hypothesis that conformational abnormalities in wild-type SOD1 can underlie SALS pathogenesis. In addition, functional experiments in isolated squid axoplasm revealed that misfolded wild-type SOD1 species inhibit conventional kinesin-based fast axonal transport (FAT) through a mechanism involving p38 kinase activation. These results provide evidence for a previously unknown SOD1-dependent pathogenic mechanism that impairs axonal transport in both FALS and SALS.

RESULTS

Oxidized and mutant SOD1 are conformationally similar

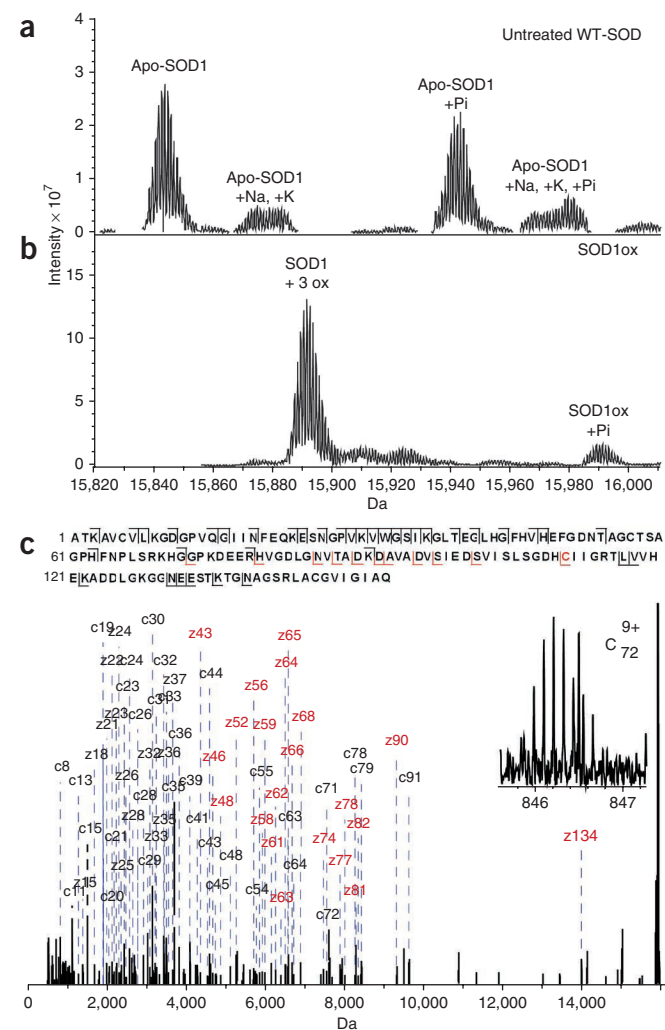
The misfolded SOD1 conformation-specific C4F6 monoclonal antibody, generated against the apo-SOD1 G93A antigen^{20,22}, reacts with multiple FALS-linked mutant SOD1, but not wild-type SOD1 proteins²⁰. When normal post-translational modifications of wild-type SOD1 are altered or when new modifications (oxidation) are introduced, wild-type SOD1 acquires some of the properties observed for FALS-linked SOD1 mutants, such as an enhanced propensity to misfold^{11,16–18}. From these observations, we hypothesized that C4F6 may recognize aberrantly modified forms of wild-type SOD1 and could therefore be used as a tool to investigate the association of such species with SALS *in vivo*.

To test this hypothesis, we exposed wild-type SOD1 to hydrogen peroxide (H₂O₂) to generate an oxidized form of wild-type SOD1 (SOD1ox). Fourier-transform mass spectrometry (FT-MS) was employed to confirm the oxidation of wild-type SOD1 (Fig. 1), as indicated by an increase of 48 Da for the predominant species in the spectrum of SOD1ox (monoisotopic mass of 15,892 Da; Fig. 1b) compared with unmodified wild-type SOD1 (15,844 Da; Fig. 1a). SOD1ox was subjected to electron capture dissociation (ECD), which confirmed that the sulfhydryl group of Cys 111 encoded in exon 4 (Fig. 2) was fully and irreversibly oxidized to sulfonic acid²³ through the incorporation of three oxygen molecules (Fig. 1c and Supplementary Table 1). No other oxidated forms of wild-type SOD1 were observed.

Figure 1 Mass spectrometry confirms the oxidation of wild-type SOD1 on exposure to hydrogen peroxide (H₂O₂). (a,b) The FT-MS spectra for untreated wild-type SOD1 (a) and oxidized wild-type SOD1 (SOD1ox, b). The data shown here have been automatically deconvoluted and reconstructed into a mass domain. The conditions under which the FT-MS analysis was performed reduced the integrity of the SOD1 dimer interface and the SOD1 metal-binding capacity (a). Thus, the apo form of wild-type SOD1 (15,844 Da, average nominal mass) was the predominate species in the mass spectrum of unmodified wild-type SOD1. Peaks representing SOD1 adducts containing sodium, potassium and phosphate ions from the buffers employed during the purification of SOD1 are indicated. The predominant species in the SOD1ox spectrum had a mass increase of 48 Da (15,892 Da) relative to apo-SOD1, which corresponds to the incorporation of three oxygens (+3ox, +48 Da) (b). (c) SOD1 proteins were subjected to gas-phase isolation followed by ECD (shown for SOD1ox). MS/MS fragments were assigned using monoisotopic masses with a 5 ppm cutoff and superimposed on the SOD1 primary sequence (top), where γ indicates unmodified c-type fragment ions that include the N terminus, L indicates unmodified z-type fragment ions that include the C terminus and the red L indicates +48 Da modified z-type fragment ions corresponding to the conversion of the sulfhydryl group at Cys 111 into sulfonic acid (+3ox). Inset shows raw data for c₇₂⁹⁺ fragment. The SOD1ox peptides resulting from ECD that were used to deduce the Cys111 site of oxidation are shown in Supplementary Table 1.

A series of western immunoblot analyses were performed to address the specificity and reactivity of the conformation specific C4F6 antibody (Fig. 3). A native western analysis revealed that C4F6 was selective for recombinant SOD1ox, as compared with untreated wild-type SOD1 protein. The commercially available monoclonal SDG6 antibody, which is reactive for the native form of SOD1, recognized both SOD1ox and wild-type SOD1 (Fig. 3a). SOD1ox migrated as a relatively diffuse band, indicative of a heterogeneous population of SOD1 molecules that migrate with both slower and faster motilities relative to untreated wild-type SOD1 (ref. 24). The migration patterns of SOD1ox may be attributed to a loss of hydrodynamic volume as a result of misfolding (slower mobility), loss or exchange of metals (faster mobility), and/or a shift in the monomer-dimer equilibrium toward the monomer (faster mobility)²⁵. As expected, C4F6 reacted to mutant SOD1 G93A, but not wild-type SOD1, by a native western analysis of tissue lysates derived from the respective transgenic mice (Fig. 3b). C4F6 reacted to SOD1 G93A under denaturing conditions; however, C4F6 was no longer reactive for SOD1ox when this protein was denatured (Fig. 3c).

To address whether oxidation of Cys111 is necessary for detection by the C4F6 antibody under native conditions, we performed the native western analysis described above with the SOD1 mutant containing C6A/C111S point mutations (AS-SOD1)²⁶. In contrast to wild-type SOD1, there was no evidence of AS-SOD1



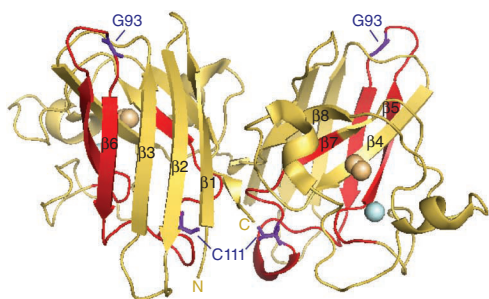


Figure 2 The structure of wild-type SOD1. The X-ray crystallographic structure of wild-type SOD1 (Protein database, accession #2C9V)⁴⁸ is shown, modeled in PyMOL. Wild-type SOD1 residues G93 and C111 in exon 2 are highlighted and labeled in purple. The zinc and copper atoms are shown in cyan and orange, respectively. SOD1 conformation-specific antibodies epitope mapped to the following regions: C4F6 to exon 4 (residues H80–V118 highlighted in red), A9G3 (Fig. 4c) to exons 1 and 2 (comprised of β strands 1–4), SEDI³⁸ to β strand 8 and USOD³³ to β strand 4.

oxidation as a result of H_2O_2 treatment, nor was C4F6 reactive for H_2O_2 -treated AS-SOD1 (Supplementary Fig. 1). Therefore, oxidation of Cys111 is required for the observed reactivity of C4F6 for SOD1ox.

The C4F6 reactive epitope, which is present in both SOD1 G93A and SOD1ox, was further investigated in an epitope mapping analysis. We transfected GST-tagged constructs encoding either the full-length SOD1-G93A gene or SOD1-G93A lacking one of the five SOD1 exons into HEK-293 cells and used the cell lysates for western blot analysis with C4F6. C4F6 reactivity required the presence of exon 4 in GST-SOD1 G93A (Fig. 3e), which harbors the G93→A mutation (Fig. 2). As expected, C4F6 was not reactive toward endogenous wild-type SOD1, whereas a commercial polyclonal antibody to SOD1 reacted to all of the SOD1 proteins (Fig. 3e).

The fact that C4F6 only recognized SOD1ox in the native conformation indicates that there is a conformational epitope in SODox, rather than the sulfonic moiety at Cys111, that is recognized by C4F6. Moreover, C4F6 is reactive for other FALS-linked SOD1 proteins, in addition to SOD1 G93A, under native conditions²⁰, but this antibody detected SOD1 G93A and not SOD1 G93C, G93D, G93R, G93S or G93V under denaturing conditions (Fig. 3d). Collectively, these

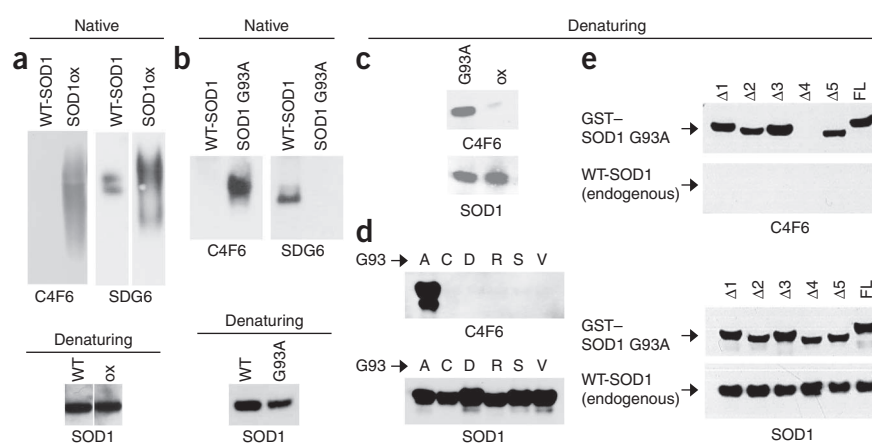
data indicate that C4F6 recognizes an epitope in SOD1 G93A that contains both a conformational component and the G93A sequence component. The formation of this conformational epitope was induced by both the G93→A mutation and the Cys111 sulfonic acid moiety (Fig. 3), both of which are in exon 4 (Fig. 2). However, the conformational component of the epitope was lost when the SOD1 proteins were denatured, leaving only the G93A sequence element of the epitope to confer C4F6 reactivity (Fig. 3c,e).

SOD1ox inhibits kinesin-based fast axonal transport

Immunochemical analysis of wild-type SOD1, SOD1ox and FALS-linked SOD1 mutants with the C4F6 antibody suggested that there was a common conformational change shared by FALS-linked SOD1 mutants and SOD1ox. These observations prompted us to compare the effects of SOD1ox with FALS-linked SOD1 mutant proteins in an ALS-relevant biological assay. We carried out vesicle motility assays in isolated squid axoplasm and found that the FALS-linked SOD1 H46R mutant selectively inhibited conventional kinesin-based fast axonal transport (FAT) in the anterograde direction (Fig. 4a), whereas the wild-type SOD1 protein did not affect FAT in either the anterograde or retrograde directions (Fig. 4b; G.M. and S.T.B., unpublished observations, and ref. 10). This experimental system allows for quantitative analysis of membrane-bound organelles moving in both anterograde (conventional kinesin dependent) and retrograde (cytoplasmic dynein dependent) directions^{27,28}. Furthermore, the lack of plasma membrane in this preparation facilitates direct evaluation of the effects of neuropathogenic proteins on FAT^{29,30}. Isolation of the squid axoplasm from the cell body and removal of plasma membrane allows one to investigate the effect of small molecules and proteins on FAT in a transcription-independent manner. We perfused SOD1ox (5 μ M) into isolated axoplasm, where it selectively inhibited anterograde FAT (Fig. 4c) to a similar extent as the SOD1 H46R mutant. Thus, SOD1ox mimics the toxic effect of the FALS-linked SOD1 mutant in these assays.

Phosphorylation of the molecular motor conventional kinesin is known to regulate FAT *in vivo*¹⁰. Furthermore, FALS-linked mutant SOD1 inhibits FAT by a mechanism involving the activation of a kinase pathway (G.M. and S.T.B., unpublished observations, and ref. 10). To evaluate the possibility that SOD1ox-mediated inhibition of anterograde FAT also involves the activation of axonal kinases,

Figure 3 The C4F6 monoclonal antibody reacts with a conformational epitope shared by SOD1ox and mutant SOD1. (a) Recombinant SOD1ox and wild-type SOD1 (6 μ g per lane) were subjected to a western analysis using native (nondenaturing) gels with the C4F6 and SDG6 monoclonal antibodies. Native SOD1ox, but not wild-type SOD1, was detected by C4F6, whereas SDG6 was reactive for both proteins. The samples were diluted (1 ng per lane) and subjected to an SDS (denaturing) western analysis with a polyclonal anti-SOD1 antibody (binding site) to demonstrate equal gel loading. (b) The native western blot revealed that C4F6 only reacted to native SOD1 G93A, whereas SDG6 only reacted to native wild-type SOD1 in lysates (30 μ g total protein per lane) that were derived from the respective transgenic mouse. The SDS (denaturing) western analysis, performed as in a, indicated that gel loading was equal. (c) C4F6 was reactive for recombinant SOD1 G93A (55 ng per lane), but not SODox (55 ng per lane), whereas a polyclonal antibody to SOD1 (Calbiochem) detected both proteins. (d) Under denaturing conditions, C4F6 was only reactive for SOD1 G93A and not for the other indicated SOD1 mutants. (e) C4F6 epitope mapped to exon 4. Lysates (30 μ g total protein) from HEK 293 mammalian cells transfected with the indicated GST-tagged construct (Δ 1–5 denote the respective exon-deleted construct; FL, full length) were probed with C4F6 or a polyclonal antibody to SOD1 (Binding Site).



The SDS (denaturing) western analysis, performed as in a, indicated that gel loading was equal. (c) C4F6 was reactive for recombinant SOD1 G93A (55 ng per lane), but not SODox (55 ng per lane), whereas a polyclonal antibody to SOD1 (Calbiochem) detected both proteins. (d) Under denaturing conditions, C4F6 was only reactive for SOD1 G93A and not for the other indicated SOD1 mutants. (e) C4F6 epitope mapped to exon 4. Lysates (30 μ g total protein) from HEK 293 mammalian cells transfected with the indicated GST-tagged construct (Δ 1–5 denote the respective exon-deleted construct; FL, full length) were probed with C4F6 or a polyclonal antibody to SOD1 (Binding Site).

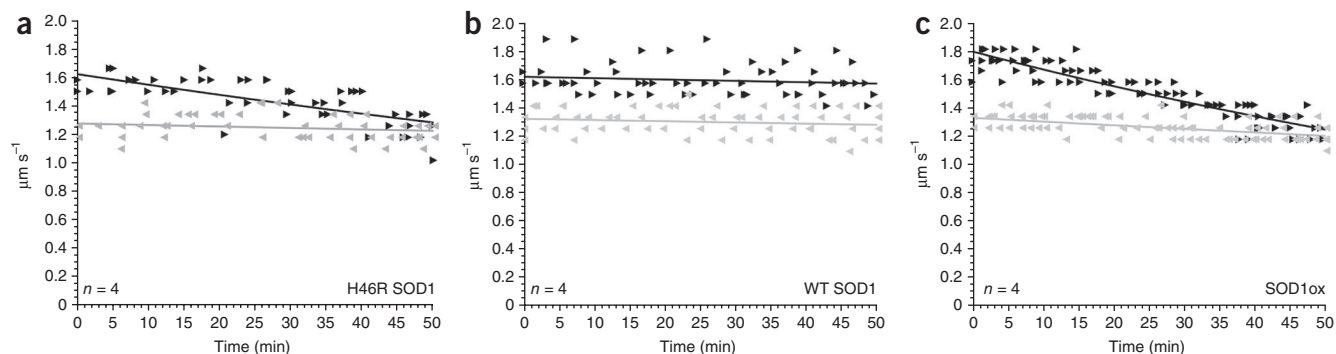


Figure 4 SOD1ox recapitulates the inhibitory effect of FALS-linked mutant SOD1 on anterograde FAT. (**a–c**) Vesicle motility assays in isolated squid axoplasm. Individual fast axonal transport (FAT) velocity ($\mu\text{m s}^{-1}$) measurements (arrowheads) are plotted as a function of time (min). Dark arrowheads and line represent anterograde, conventional kinesin-dependent FAT rates. Gray arrows and line represent retrograde, dynein-dependent FAT rates. Perfusion of $5 \mu\text{M}$ of the FALS-linked H46R mutant into squid axoplasm caused a marked reduction in the rate of anterograde FAT ($n = 4$, **a**). In contrast, perfusion of $5 \mu\text{M}$ wild-type SOD1 in the squid axoplasm had no effect on anterograde or retrograde FAT rates ($n = 4$, **b**). Perfusion of $5 \mu\text{M}$ SOD1ox mimicked the inhibitory effect of SOD1 H46R on anterograde FAT ($n = 4$, **c**).

we screened for changes in the activity of various protein kinases in axoplasms perfused with either wild-type SOD1 or SOD1ox by immunoblotting with activation-specific phosphoantibodies. No changes in the activities of GSK3 and ERK were observed between wild-type SOD1- and SOD1ox-perfused axoplasms (**Fig. 5a,b**). In contrast, antibodies specific for phosphorylated, catalytically active p38 (p-p38) revealed a marked increase in p38 activation in axoplasms perfused with SOD1ox, as compared with those perfused with wild-type SOD1 (**Fig. 5a**). Quantitative analysis of immunoblots indicated that SOD1ox induced an approximately fourfold increase in p38 activation as compared with wild-type SOD1 ($n = 6$, $P < 0.05$, **Fig. 5b**). Consistent with these data, perfusion of the highly specific p38 MAPK inhibitors SB203580 ($5 \mu\text{M}$; **Fig. 5c**)³¹ or MW01-2-069SRM ($10 \mu\text{M}$; **Fig. 5d**) with SOD1ox prevented the inhibitory effect of SOD1ox on anterograde FAT. Thus, inhibition of anterograde FAT by SOD1ox requires the activation of p38 kinase. Taken together, these data indicate that an aberrantly modified form of wild-type SOD1, which shares conformational motifs with FALS-linked SOD1 mutant proteins, inhibits conventional kinesin-based FAT through a mechanism involving p38 activation.

Misfolded SOD1 is present in SALS spinal cord tissues

To address the hypothesis that aberrantly modified forms of wild-type SOD1 are associated with SALS *in vivo*, we performed immunohistochemistry on postmortem human spinal cord (SpC) using the conformation-specific C4F6 antibody (**Fig. 6**) that reacts specifically with mutant SOD1 and SOD1ox, but not unmodified wild-type SOD1 (clinical and demographic information are presented in **Supplementary Tables 2** and **3**). In contrast with other studies that employ misfolded-SOD1 conformation-specific antibodies^{33,34}, we avoided antigen retrieval approaches that can potentially alter the antigen conformation (Online Methods). Positive C4F6 staining was observed in four of nine SALS cases (SALS1–4; **Fig. 6a,d–f**). Of the five remaining SALS cases, SpC sections from two cases showed extensive degeneration in the motor regions to the extent that motor neurons could not be detected. As the motor neurons appeared to be positively stained for C4F6 (**Fig. 6a,d–f**), we cannot exclude the possibility that these two aforementioned cases lacking detectable motor neurons would have been C4F6 positive at an earlier stage of disease. Notably, no C4F6 staining was observed in 17 control cases ($P = 0.008$, two-tailed Fisher's exact test; **Fig. 6g,h**). Lack of C4F6 immunoreactivity

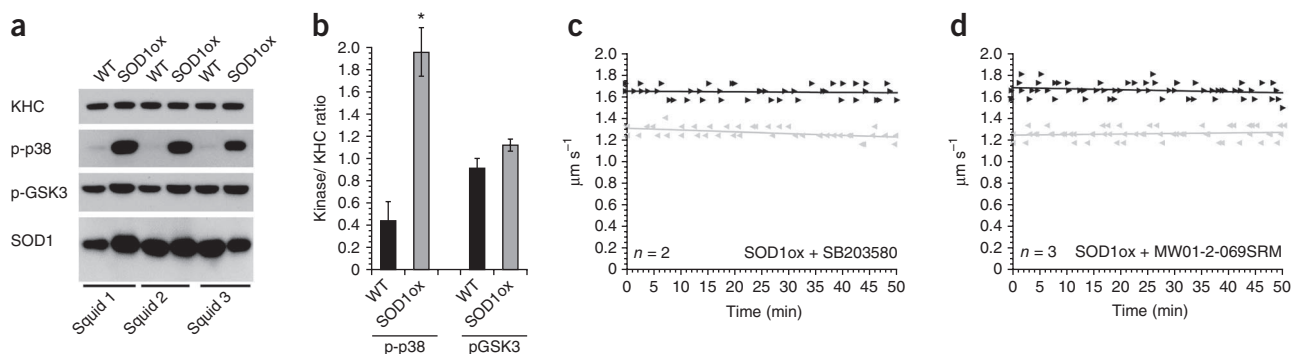


Figure 5 p38 mediates the inhibition of anterograde FAT induced by SOD1ox. (**a**) Immunoblotting analysis using activation-specific phosphoantibodies revealed a marked activation of p38 (p-p38) in axoplasms perfused with recombinant oxidized SOD1 (SOD1ox), compared to those perfused with recombinant unmodified wild-type SOD1 (WT). In contrast, no changes were found in the activities of ERK (pERK) and GSK3 (pGSK3) in association with a specific SOD1 species. A monoclonal antibody against SOD1 (D3H5)²² confirmed similar levels of SOD1 perfusion, and antibodies to kinesin-1 (KHC) provided a loading control for total levels of axoplasmic protein. Results from three independent experiments are shown (Squid 1–3). (**b**) Quantification of results in **a** reveals an approximately fourfold increase in the phosphorylation of p38 (indicative of p38 activation) in SOD1ox-perfused axoplasms, compared to unmodified wild-type SOD1-perfused axoplasms ($n = 6$, $*P < 0.05$ by the pooled t test of $\mu 1$ – $\mu 2$). Error bars reflect the standard error of multiple measurements. Co-perfusion of the highly specific p38 inhibitors SB203580 (**c**) and MW01-2-069SRM (**d**) blocked the inhibitory effect of SOD1ox on anterograde FAT (compare to **Fig. 4c**). Similarly, FALS-linked mutant SOD1 polypeptides inhibit anterograde FAT through a mechanism involving activation of p38 kinase (G.M. and S.T.B., unpublished observations, and ref. 10).

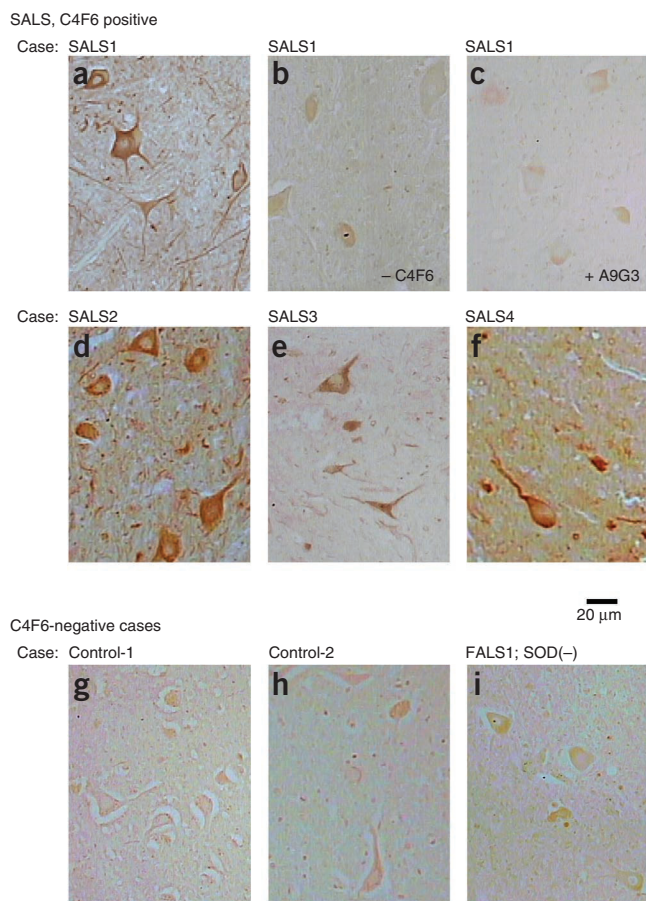


Figure 6 The C4F6 monoclonal antibody is reactive for wild-type SOD1 in SALS tissues. (a) C4F6 positive staining is shown for a SALS case (SALS1). (b,c) The positive staining observed for SALS1 was lost when C4F6 was excluded from the staining protocol (b) or when the alternative SOD1-mutant specific A9G3 antibody was employed (c). (d–f) C4F6 positive staining is shown for three SALS cases (SALS2–4). (g–i) Representative control cases (g,h) and an SOD1-negative FALS case (i) showing the lack of positive C4F6 reactivity for such cases. In total, four out of nine SALS cases exhibited positive C4F6 staining, whereas 0 of 17 control cases exhibited positive staining. For clinical and demographic information on these cases, see **Supplementary Tables 2 and 3**.

case (**Fig. 6c**). Thus, the wild-type SOD1 present in our C4F6-positive SALS cases exposed a specific epitope that was not detectable by all misfolded SOD1 conformation-specific antibodies, consistent with other reports of misfolded SOD1 conformation-specific antibodies that epitope map outside the region encoded by exon 4 (refs. 33,34).

Aggregated wild-type SOD1 is immunohistochemically detected in the Lewy body-like hyaline inclusions of some^{35,36}, but not all³⁷, SALS cases. To assess the levels of aggregated wild-type SOD1 in our C4F6-positive SALS cases (SALS1–4), we extracted insoluble SOD1 from our tissue lysates derived from frozen, postmortem human SpC tissue. The protocol was first validated with tissue lysates derived from transgenic G93A and naive mice. As expected, immunoblot analysis detected insoluble SOD1 in the tissue lysates of SOD1 G93A mice⁴, but not in those of naive mice (**Supplementary Fig. 2**). The levels of insoluble SOD1 extracted from human tissues were not substantially different between human ALS cases and controls (**Supplementary Fig. 2**). The diffuse staining patterns of C4F6 and the pan polyclonal antibody to SOD1 (**Supplementary Fig. 3**) observed in SALS cases, together with the lack of evidence for elevated levels of insoluble wild-type SOD1, suggested that the misfolded wild-type SOD1 species in SALS1–4 cases are relatively soluble. However, we cannot exclude the possibility that smaller oligomeric aggregates may be present or that SOD1 aggregates could be detected with other antibodies to SOD1 that reportedly detect such species^{33,38}.

The immunohistochemistry analysis described above suggests that misfolded, C4F6-positive, wild-type SOD1 was significantly ($P < 0.05$) associated with many SALS cases. We evaluated the possibility that endogenous misfolded wild-type SOD1 from SpC tissue inhibits FAT as observed with SOD1ox (**Fig. 4c**). To this end, we immunopurified wild-type SOD1 from both SALS and control SpC

in a FALS case without SOD1 mutations confirmed the specificity of staining (**Fig. 6i**). We note that the optimal immunohistochemistry staining results were obtained with paraffin-fixed tissue, whereas immunohistochemistry of frozen tissue specimens generally did not reveal strong C4F6 staining (Online Methods).

The SOD1 mutant-specific A9G3 monoclonal antibody (J.-P.J., unpublished data), which was also generated against SOD1 G93A²⁰, but epitope mapped to regions encoded by exons 1 and 2 (D.A.B., unpublished data), did not react to wild-type SOD1 in the SALS1

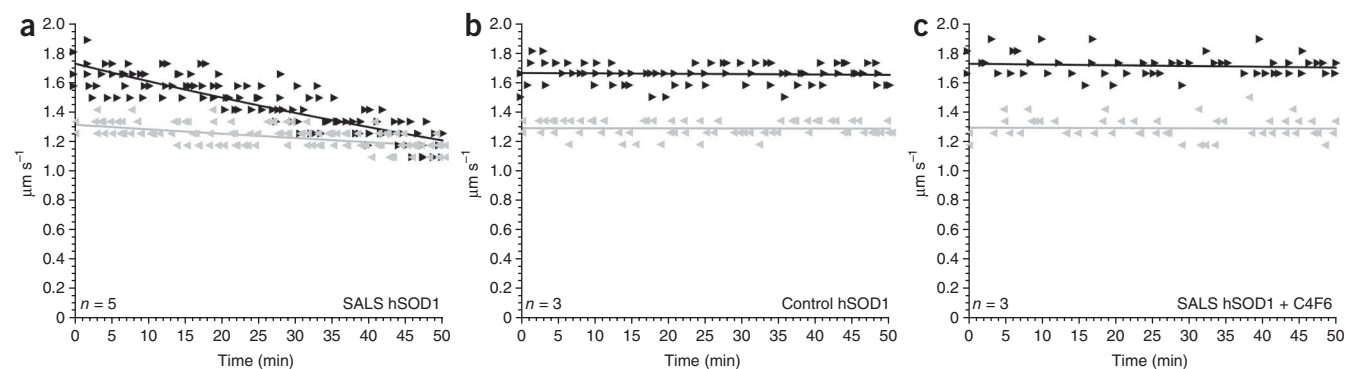


Figure 7 Wild-type SOD1 purified from SALS tissues inhibits anterograde FAT. hSOD1 immunopurified from SpCs of SALS (SALS hSOD1) and control (Ctrl hSOD1) were perfused into isolated squid axoplasm and the effects on FAT were evaluated as in **Figure 4**. (a) Perfusion of SALS-derived hSOD1 (1 μM) selectively inhibited anterograde FAT (dark lines, right arrowheads) while retrograde FAT (gray lines, left arrowheads) remained unchanged ($n = 5$ motility plots from 2 independent immunopurifications of hSOD1). The inhibitory effect of SALS-derived hSOD1 on FAT mimicked that of FALS-SOD1 H46R and SOD1ox (**Fig. 4**). (b) Perfusion of control-derived hSOD1 had no effect on FAT ($n = 3$ motility plots from 2 independent immunopurifications). (c) Co-perfusion of the C4F6 monoclonal antibody (22.5 ng) with SALS-derived hSOD1 blocked the inhibitory effect of SOD1 on anterograde FAT ($n = 3$ axoplasms), demonstrating that the C4F6-reactive SOD1 species mediate the inhibitory effect on FAT.

tissues under detergent-free conditions (Online Methods) and perfused the SOD1 proteins into isolated squid axoplasm (Fig. 7). Mass spectrometry confirmed that the purified SOD1 preparations were 99% free of contaminating proteins. Perfusion of wild-type SOD1 (1 μ M) immunopurified from SALS tissues selectively inhibited anterograde FAT, but not retrograde FAT, a pattern of FAT inhibition that is consistent with that induced by both FALS-linked mutant SOD1 (Fig. 4a; G.M. and S.T.B., unpublished observations, and ref. 10) and SOD1ox (Fig. 4c). In contrast, wild-type SOD1 immunopurified from control tissues had no effect on FAT (Fig. 7b). Co-perfusion of the conformation-specific C4F6 monoclonal antibody (22.5 ng) blocked the inhibitory effect of SALS-derived SOD1 (Fig. 7c), indicating that C4F6-reactive SOD1 species mediate the inhibitory effect on FAT. The fact that mild, detergent-free conditions (Online Methods) were employed to immunopurify wild-type SOD1 proteins from human SpC lysates further suggests that the toxic, SALS-derived wild-type SOD1 species are relatively soluble.

DISCUSSION

Approximately 150 mutations dispersed throughout the SOD1 sequence have been linked to FALS (<http://alsod.iop.kcl.ac.uk/>). In many cases, these represent subtle, conservative (for example, Gly \rightarrow Ala) amino acid substitutions³; nonetheless, all of these mutations lead to an ALS phenotype. Although pathogenic mechanisms underlying FALS-linked SOD1-mediated toxicity have not been definitively elucidated, a prevailing hypothesis is that FALS-linked mutations induce an altered or misfolded conformation in SOD1 (refs. 4,5,7–9) that modifies its interactions with other proteins and perturbs its cellular localization^{39–41}.

Given the common pathological effects of diverse FALS-linked SOD1 mutations, it seems plausible that alterations to the non-Mendelian, post-translational modifications of SOD1 may similarly lead to an ALS phenotype^{13–15}. For example, disruptions of the normal SOD1 post-translational modifications (Fig. 2), such as subunit dimerization, the intrasubunit disulfide bond between residues Cys57 and Cys146, and the coordination of copper and zinc, have all been shown to cause wild-type SOD1 to aggregate^{16,17,25,38,42}. Moreover, aberrant post-translational modifications of SOD1, such as oxidation, have adverse effects on wild-type SOD1 protein conformation^{11,15,18}. Using the C4F6 monoclonal antibody²⁰, we found that both oxidation of Cys111 (Fig. 1) and mutagenesis of G93 \rightarrow A induced the formation of a conformational epitope that includes elements of exon 4 (Fig. 2) and that is not normally exposed by wild-type SOD1 (Fig. 3). In addition to this conformational component of the C4F6 epitope that is shared by SOD1ox and SOD1 G93A, there is an amino acid sequence component that includes G93A, which could be expected, as the SOD1 G93A antigen was used to raise the C4F6 antibody²⁰, and likely explains the stronger reactivity of C4F6 for G93A relative to SOD1ox under native conditions (Supplementary Fig. 1). Under denaturing conditions, the conformational epitope is lost and only the G93A sequence element remains to confer reactivity with C4F6, thus explaining a lack of C4F6 reactivity for SOD1ox and other G93 variants under denaturing conditions (Fig. 3c,e).

We examined human SpC tissues with C4F6 and found aberrantly folded wild-type SOD1 species in approximately half of the available SALS cases, but not in control cases (Fig. 6). These results indicate that at least a subset of SALS cases contain wild-type SOD1 proteins that are structurally similar to FALS-linked SOD1 mutant proteins. The lack of C4F6 reactivity in the remaining SALS cases may indicate that misfolded SOD1 is not associated with ALS pathogenesis in these cases, suggesting that modified wild-type SOD1 is involved in a subset

of SALS in an analogous manner to that of mutant SOD1 in a subset of FALS. However, we cannot confirm that the C4F6 antibody is reactive for all possible misfolded forms of wild-type SOD1.

Our finding that misfolded SOD1 was associated with SALS is consistent with the report that an aberrant 32-kDa, SOD1-containing species is indirectly detected through a biotinylation cross-linking reaction with homogenized tissue lysates from both SALS and FALS¹². We probed for a misfolded SOD1 conformation in SALS using an immunohistochemistry approach on fixed tissues with C4F6, a conformation-specific monoclonal antibody. Moreover, we found that these misfolded wild-type SOD1 species derived from C4F6-positive SALS cases recapitulate the toxic effect of FALS-linked mutant SOD1 on FAT (Fig. 7). Furthermore, we found that activation of p38 MAPK is a common feature of both SALS- and FALS-linked SOD1 inhibition of FAT (Fig. 5 and ref. 10).

Although we found that C4F6 reacts to an oxidized form of wild-type SOD1 (Fig. 3a), it is possible that other modifications to wild-type SOD1, including alterations in normal post-translational modifications^{16,17,25,38}, might also induce an altered conformation that confers C4F6 reactivity. That different modifications to SOD1 can induce similar structural consequences is supported by observations that C4F6 reacts with different FALS-linked SOD1 mutants²⁰ and by a recent hydrogen/deuterium exchange study that found enhanced flexibility in the same SOD1 electrostatic loop region (residues 133–144, located between β -strands 7 and 8; Fig. 2) for a panel of 13 different FALS-linked SOD1 mutants⁷. Additional studies with alternate misfolded forms of wild-type SOD1 and different SOD1 conformation specific antibodies will provide greater insight into the conformational similarities of these proteins and their prevalence in SALS.

Although the C4F6 antibody recognizes a conformation-dependent epitope common to both mutant and wild-type SOD1 proteins associated with ALS pathology, the critical epitope is not detected by all of the antibodies that recognize other misfolded SOD1 species. For example, our A9G3 antibody detects a subset of FALS-linked mutant SOD1 species, but did not react with SpC sections from individuals with SALS that were immunoreactive for C4F6 (Fig. 6c). Similarly, both the SOD1 exposed dimer interface (SEDI) and unfolded SOD1 (USOD) antibodies failed to detect wild-type SOD1 in SALS cases^{33,34}. There are several distinctions between the epitopes recognized by C4F6 and the SEDI and USOD antibodies. C4F6 is reactive for a conformational epitope that includes G93 encoded in exon 4 (Fig. 3), which is distal to those epitopes recognized by SEDI and USOD (Fig. 2). Moreover, both SEDI and USOD are reactive for linear sequences that can become exposed in aggregated SOD1 inclusions in FALS cases, whereas the misfolded wild-type SOD1 species in our SALS cases is relatively soluble, as evidenced by the diffuse C4F6 staining pattern (Fig. 6), the low levels of insoluble wild-type SOD1 detected in our SALS cases (Supplementary Fig. 2) and the fact that we were able to purify these species under detergent-free conditions while maintaining their inhibitory effect on anterograde FAT (Fig. 7). Notably, our immunohistochemistry methods do not require the harsh conditions used for antigen retrieval. Such treatments may disrupt the C4F6-like conformational epitope, but enhance the detection of epitopes such as those for the SEDI and USOD antibodies that are otherwise buried^{33,34}. Thus, the different findings obtained with the C4F6, SEDI and USOD antibodies are likely a result of the different epitopes recognized by these antibodies.

Our analyses of immunoreactivity patterns for the C4F6 antibody reveal that genetic variants transmitted as Mendelian traits and non-inherited modifications to SOD1 can both induce similar structural perturbations within the protein and that non-inherited modifications

of SOD1 can be associated with SALS. A critical question that follows directly from these observations is whether these SALS-linked modifications confer on wild-type SOD1 the same toxic properties that are elicited by FALS-linked SOD1 mutations, including activation of p38 and inhibition of FAT. Both recombinant SOD1ox (Fig. 4c) and wild-type SOD1 derived from C4F6-positive SALS SpC tissues (Fig. 7a) recapitulated this pattern of mutant SOD1-mediated FAT inhibition, whereas untreated recombinant wild-type SOD1 and wild-type SOD1 derived from control SpC tissues had no effect (Figs. 4b and 7b, respectively). The effect of SOD1 from C4F6-positive SALS SpC on anterograde FAT was abolished by incubation with the C4F6 antibody before perfusion (Fig. 7c). C4F6 also abolished the ability of FALS mutant SOD1 to inhibit FAT (data not shown). Biochemical and pharmacological experiments further indicated that the inhibition of anterograde FAT induced by SOD1ox involves activation of p38 kinase (Fig. 5). FALS-linked mutant SOD1-mediated defects in axonal transport have been reported previously^{10,43,44} and were thought to represent an early pathogenic event in mutant SOD1 transgenic mice that contributes to a 'dying back' mode of motor neuron degeneration^{45,46,47}. That the inhibition of FAT occurs selectively in the anterograde direction suggests that this effect of mutant SOD1 and SOD1ox is specific, as this effect is not universally observed for all toxic, neurodegenerative disease-associated proteins¹⁰. The pattern of FAT inhibition is largely determined by the nature of the regulatory kinases that become activated by the toxic protein¹⁰. Both modified wild-type SOD1 (Fig. 5) and several mutant SOD1 proteins (G.M. and S.T.B., unpublished observations, and ref. 10) inhibited FAT through a mechanism involving specific activation of p38 MAPK.

Concurrent studies have found that p38 directly phosphorylates kinesin-1 subunits of conventional kinesin and markedly inhibits the translocation of this motor protein along axonal microtubules, thereby providing a common molecular basis for the effects of activated p38 kinase activity on anterograde FAT¹⁰ (G.M. and S.T.B., unpublished observations). Thus, SALS-associated wild-type SOD1 species induce the same defects on conventional kinesin-based FAT as FALS-linked SOD1 mutants and by the same molecular mechanism.

The idea that proteins can become pathogenic via both inheritable and non-heritable modifications has precedence in the context of other neurodegenerative diseases, as exemplified by α -synuclein in Parkinson's disease and A β or tau in Alzheimer's disease and frontotemporal dementia (FTDP). Although our data do not rule out potential toxic effects of aggregated wild-type SOD1 species in ALS pathogenesis, they reveal toxic effects associated with relatively soluble, misfolded wild-type SOD1 species in SALS. Although aberrantly modified wild-type SOD1 is prone to aggregation *in vitro*^{16,17,25,38}, the toxic species *in vivo* may actually be a pre-aggregated, conformationally mis-folded form of the protein.

In conclusion, we found that misfolded, SALS-linked wild-type SOD1 proteins activate the same neurotoxic mechanism that is invoked by FALS-linked SOD1 mutants, strongly suggesting that conformational abnormalities and post-translational modifications in wild-type SOD1 can contribute to SALS pathogenesis. Our results identify a pathogenic mechanism for ALS that is common to both mutant SOD1-mediated FALS and many cases of SALS.

METHODS

Methods and any associated references are available in the online version of the paper at <http://www.nature.com/natureneuroscience/>.

Note: Supplementary information is available on the Nature Neuroscience website.

ACKNOWLEDGMENTS

We are grateful to J. Landers and P. Sapp for DNA sequencing analysis of the SALS cases employed in this study, L. Hayward, A. Tiwari and R.-J. Chain for help with expression of recombinant wild-type SOD1, S. Berth, A. Leitman and M. Sapauskaitė for help with axoplasm vesicle transport assays, A. Kaminska and L. Molla for help with biochemical experiments in squid axoplasm, M. Prudencio and D. Borchelt for cell lysates containing SOD1 G93 mutants, C. Vanderburg, E. Tamrazian, A. Bialik and the Diabetes and Endocrinology Research Center (University of Massachusetts Medical Center) for assistance with immunohistochemistry, K. Fitch and the Massachusetts Alzheimer Disease Research Center (P50AG005134) for assistance with human tissue samples, J. Zitzewitz for C6A/C111S-SOD1 protein, A. Weiss for assistance with mice, K. Green at the University of Massachusetts Medical Center Proteomics and Mass Spectrometry Facility for analysis of C6A/C111S-SOD1, and G. Petsko for insightful dialogue and support. We acknowledge financial support from the ALS Therapy Alliance-CVS Pharmacy (D.A.B. and G.M.), 2007/2008 Marine Biological Laboratory research fellowships (G.M.), the ALS Association (D.A.B., R.H.B. Jr, G.M. and S.T.B.), the US National Institutes of Health (D.A.B. (National Institute on Neurological Disorders and Stroke, RO1NS067206-01), R.H.B. Jr (National Institute on Neurological Disorders and Stroke, U01NS05225-03, RO1NS050557-05, 1RC1NS068391-01 and 1RC2NS070342-01), S.T.B. and J.N.A.), Canadian Institutes of Health Research (J.-P.J.), the Angel Fund (R.H.B. Jr) and Project ALS (R.H.B. Jr).

AUTHOR CONTRIBUTIONS

D.A.B., G.M., S.T.B. and R.H.B. Jr wrote the manuscript. D.A.B. prepared recombinant and immunopurified SOD1 proteins. G.M., Y.S. and S.T.B. performed vesicle motility assays and biochemical experiments in isolated squid axoplasm. N.M.K. and J.N.A. performed the mass spectrometry. F.G.-L. and J.-P.J. prepared the mutant-specific antibodies. P.P. made the SOD1 exon deleted constructs. H.G., D.M.-Y. and M.P.F. provided human tissues for staining. D.A.B., B.A.F. and N.L. performed western analyses. All of the authors reviewed and edited the manuscript.

COMPETING FINANCIAL INTERESTS

The authors declare no competing financial interests.

Published online at <http://www.nature.com/natureneuroscience/>.

Reprints and permissions information is available online at <http://www.nature.com/reprintsandpermissions/>.

- Tandan, R. & Bradley, W.G. Amyotrophic lateral sclerosis. Part 1. Clinical features, pathology, and ethical issues in management. *Ann. Neurol.* **18**, 271–280 (1985).
- Valdmanis, P.N., Daoud, H., Dion, P.A. & Rouleau, G.A. Recent advances in the genetics of amyotrophic lateral sclerosis. *Curr. Neurol. Neurosci. Rep.* **9**, 198–205 (2009).
- Valentine, J.S., Doucette, P.A. & Zittin Potter, S. Copper-zinc superoxide dismutase and amyotrophic lateral sclerosis. *Annu. Rev. Biochem.* **74**, 563–593 (2005).
- Bruijn, L.I. *et al.* Aggregation and motor neuron toxicity of an ALS-linked SOD1 mutant independent from wild-type SOD1. *Science* **281**, 1851–1854 (1998).
- Chattopadhyay, M. & Valentine, J.S. Aggregation of copper-zinc superoxide dismutase in familial and sporadic ALS. *Antioxid. Redox. Signal* **11**, 1603–1614 (2009).
- Furukawa, Y., Fu, R., Deng, H.X., Siddique, T. & O'Halloran, T.V. Disulfide cross-linked protein represents a significant fraction of ALS-associated Cu, Zn-superoxide dismutase aggregates in spinal cords of model mice. *Proc. Natl. Acad. Sci. USA* **103**, 7148–7153 (2006).
- Molnar, K.S. *et al.* A common property of amyotrophic lateral sclerosis-associated variants: destabilization of the Cu/Zn superoxide dismutase electrostatic loop. *J. Biol. Chem.* **284**, 30965–30973 (2009).
- Prudencio, M., Hart, P.J., Borchelt, D.R. & Andersen, P.M. Variation in aggregation propensities among ALS-associated variants of SOD1: correlation to human disease. *Hum. Mol. Genet.* **18**, 3217–3226 (2009).
- Wang, Q., Johnson, J.L., Agar, N.Y. & Agar, J.N. Protein aggregation and protein instability govern familial amyotrophic lateral sclerosis patient survival. *PLoS Biol.* **6**, e170 (2008).
- Morfini, G.A. *et al.* Axonal transport defects in neurodegenerative diseases. *J. Neurosci.* **29**, 12776–12786 (2009).
- Ezzi, S.A., Urushitani, M. & Julien, J.P. Wild-type superoxide dismutase acquires binding and toxic properties of ALS-linked mutant forms through oxidation. *J. Neurochem.* **102**, 170–178 (2007).
- Gruzman, A. *et al.* Common molecular signature in SOD1 for both sporadic and familial amyotrophic lateral sclerosis. *Proc. Natl. Acad. Sci. USA* **104**, 12524–12529 (2007).
- Beckman, J.S., Estevez, A.G., Crow, J.P. & Barbeito, L. Superoxide dismutase and the death of motoneurons in ALS. *Trends Neurosci.* **24**, S15–S20 (2001).
- Bredesen, D.E., Ellerby, L.M., Hart, P.J., Wiedau-Pazos, M. & Valentine, J.S. Do posttranslational modifications of CuZnSOD lead to sporadic amyotrophic lateral sclerosis? *Ann. Neurol.* **42**, 135–137 (1997).
- Kabashi, E., Valdmanis, P.N., Dion, P. & Rouleau, G.A. Oxidized/misfolded superoxide dismutase-1: the cause of all amyotrophic lateral sclerosis? *Ann. Neurol.* **62**, 553–559 (2007).

16. Durazo, A. *et al.* Metal-free superoxide dismutase-1 and three different ALS variants share a similar partially unfolded (beta)-barrel at physiological temperature. *J. Biol. Chem.* **277**, 15923–15931 (2009).
17. Estévez, A.G. *et al.* Induction of nitric oxide-dependent apoptosis in motor neurons by zinc-deficient superoxide dismutase. *Science* **286**, 2498–2500 (1999).
18. Rakhit, R. *et al.* Oxidation-induced misfolding and aggregation of superoxide dismutase and its implications for amyotrophic lateral sclerosis. *J. Biol. Chem.* **277**, 47551–47556 (2002).
19. Banci, L. *et al.* Metal-free superoxide dismutase forms soluble oligomers under physiological conditions: a possible general mechanism for familial ALS. *Proc. Natl. Acad. Sci. USA* **104**, 11263–11267 (2007).
20. Urushitani, M., Ezzi, S.A. & Julien, J.P. Therapeutic effects of immunization with mutant superoxide dismutase in mice models of amyotrophic lateral sclerosis. *Proc. Natl. Acad. Sci. USA* **104**, 2495–2500 (2007).
21. Brady, S.T., Lasek, R.J. & Allen, R.D. Fast axonal transport in extruded axoplasm from squid giant axon. *Science* **218**, 1129–1131 (1982).
22. Gros-Louis, F., Soucy, G., Larivière, R. & Julien, J.P. Intracerebroventricular infusion of monoclonal antibody or its derived Fab fragment against misfolded forms of SOD1 mutant delays mortality in a mouse model of ALS. *J. Neurochem.* **113**, 1188–1199 (2010).
23. Fujiwara, N. *et al.* Oxidative modification to cysteine sulfonic acid of Cys111 in human copper-zinc superoxide dismutase. *J. Biol. Chem.* **282**, 35933–35944 (2007).
24. Tiwari, A. *et al.* Metal deficiency increases aberrant hydrophobicity of mutant superoxide dismutases that cause amyotrophic lateral sclerosis. *J. Biol. Chem.* **284**, 27746–27758 (2009).
25. Rakhit, R. *et al.* Monomeric Cu,Zn-superoxide dismutase is a common misfolding intermediate in the oxidation models of sporadic and familial amyotrophic lateral sclerosis. *J. Biol. Chem.* **279**, 15499–15504 (2004).
26. Svensson, A.K., Bilsel, O., Kondrashkina, E., Zitzewitz, J.A. & Matthews, C.R. Mapping the folding free energy surface for metal-free human Cu,Zn superoxide dismutase. *J. Mol. Biol.* **364**, 1084–1102 (2006).
27. Brady, S.T., Lasek, R.J. & Allen, R.D. Video microscopy of fast axonal transport in extruded axoplasm: a new model for study of molecular mechanisms. *Cell Motil.* **5**, 81–101 (1985).
28. Morfini, G., Szebenyi, G., Elluru, R., Ratner, N. & Brady, S.T. Glycogen synthase kinase 3 phosphorylates kinesin light chains and negatively regulates kinesin-based motility. *EMBO J.* **21**, 281–293 (2002).
29. Morfini, G. *et al.* JNK mediates pathogenic effects of polyglutamine-expanded androgen receptor on fast axonal transport. *Nat. Neurosci.* **9**, 907–916 (2006).
30. Morfini, G.A. *et al.* Pathogenic huntingtin inhibits fast axonal transport by activating JNK3 and phosphorylating kinesin. *Nat. Neurosci.* **12**, 864–871 (2009).
31. Fabian, M.A. *et al.* A small molecule-kinase interaction map for clinical kinase inhibitors. *Nat. Biotechnol.* **23**, 329–336 (2005).
32. Munoz, L. *et al.* A novel p38 alpha MAPK inhibitor suppresses brain proinflammatory cytokine up-regulation and attenuates synaptic dysfunction and behavioral deficits in an Alzheimer's disease mouse model. *J. Neuroinflammation* **4**, 21 (2007).
33. Kerman, A. *et al.* Amyotrophic lateral sclerosis is a non-amyloid disease in which extensive misfolding of SOD1 is unique to the familial form. *Acta Neuropathol.* **119**, 335–344 (2010).
34. Liu, H.N. *et al.* Lack of evidence of monomer/misfolded superoxide dismutase-1 in sporadic amyotrophic lateral sclerosis. *Ann. Neurol.* **66**, 75–80 (2009).
35. Shibata, N., Asayama, K., Hirano, A. & Kobayashi, M. Immunohistochemical study on superoxide dismutases in spinal cords from autopsied patients with amyotrophic lateral sclerosis. *Dev. Neurosci.* **18**, 492–498 (1996).
36. Shibata, N. *et al.* Cu/Zn superoxide dismutase-like immunoreactivity in Lewy body-like inclusions of sporadic amyotrophic lateral sclerosis. *Neurosci. Lett.* **179**, 149–152 (1994).
37. Watanabe, M. *et al.* Histological evidence of protein aggregation in mutant SOD1 transgenic mice and in amyotrophic lateral sclerosis neural tissues. *Neurobiol. Dis.* **8**, 933–941 (2001).
38. Rakhit, R. *et al.* An immunological epitope selective for pathological monomer-misfolded SOD1 in ALS. *Nat. Med.* **13**, 754–759 (2007).
39. Pasinelli, P. *et al.* Amyotrophic lateral sclerosis-associated SOD1 mutant proteins bind and aggregate with Bcl-2 in spinal cord mitochondria. *Neuron* **43**, 19–30 (2004).
40. Urushitani, M. *et al.* Chromogranin-mediated secretion of mutant superoxide dismutase proteins linked to amyotrophic lateral sclerosis. *Nat. Neurosci.* **9**, 108–118 (2006).
41. Vande Velde, C., Miller, T.M., Cashman, N.R. & Cleveland, D.W. Selective association of misfolded ALS-linked mutant SOD1 with the cytoplasmic face of mitochondria. *Proc. Natl. Acad. Sci. USA* **105**, 4022–4027 (2008).
42. Lindberg, M.J., Normark, J., Holmgren, A. & Oliveberg, M. Folding of human superoxide dismutase: disulfide reduction prevents dimerization and produces marginally stable monomers. *Proc. Natl. Acad. Sci. USA* **101**, 15893–15898 (2004).
43. De Vos, K.J., Grierson, A.J., Ackerley, S. & Miller, C.C. Role of axonal transport in neurodegenerative diseases. *Annu. Rev. Neurosci.* **31**, 151–173 (2008).
44. Ström, A.L. *et al.* Retrograde axonal transport and motor neuron disease. *J. Neurochem.* **106**, 495–505 (2008).
45. Collard, J.F., Cote, F. & Julien, J.P. Defective axonal transport in a transgenic mouse model of amyotrophic lateral sclerosis. *Nature* **375**, 61–64 (1995).
46. Williamson, T.L. & Cleveland, D.W. Slowing of axonal transport is a very early event in the toxicity of ALS-linked SOD1 mutants to motor neurons. *Nat. Neurosci.* **2**, 50–56 (1999).
47. Fischer, L.R. & Glass, J.D. Axonal degeneration in motor neuron disease. *Neurodegener. Dis.* **4**, 431–442 (2007).
48. Strange, R.W. *et al.* Variable metallation of human superoxide dismutase: atomic resolution crystal structures of Cu-Zn, Zn-Zn and as-isolated wild-type enzymes. *J. Mol. Biol.* **356**, 1152–1162 (2006).

ONLINE METHODS

Antibodies and reagents. In our experiments, we used antibodies to SOD1 (PC077, the Binding Site; Calbiochem, 574597; SDG6 clone, Sigma), mutant SOD1 (C4F6 and A9G3 (ref. 20)), KHC (H2)³⁰, phospho-p38 MAPK (Cell Signaling #9215), phospho-ERK (Santa Cruz #7383) and phospho-GSK3 (Santa Cruz #11757). Secondary antibodies included horseradish peroxidase (HRP)-conjugated rabbit antibody to sheep IgG (Upstate, 12-342) and HRP-conjugated rabbit antibody to mouse IgG (Sigma, A9044). SB203580 was obtained from Calbiochem and handled as described previously³⁰, and MW01-2-069SRM was a generous gift from M. Watterson (Northwestern University). Total protein concentrations were determined using bicinchoninic acid (BCA) assay (Pierce #23225).

Human samples. Human control and SALS paraffin-embedded SpC tissues for immunohistochemistry analysis and frozen tissues for immunopurification of wild-type SOD1 were obtained through the Massachusetts Alzheimer's Disease Research Center at Massachusetts General Hospital with the appropriate Partners Healthcare IRB approval (protocol 1999-p-004325). All experiments were performed with either lumbar or thoracic SpC tissue sections. All available demographics and clinical information for the SALS and control cases analyzed throughout this study are presented in **Supplementary Tables 1 and 2**.

Immunoblots. Samples for native western analysis were prepared with 2× loading buffer (Invitrogen, LC2673), separated by PAGE with 12% Tris-glycine gels (Invitrogen, EC60052BOX) in Tris-glycine buffer (Invitrogen, LC2672) for 3 h at 4 °C and transferred to PVDF (Pierce #88518) in transfer buffer, pH 9.2 (Invitrogen, LC3675) for 90 min at 4 °C. Membranes were fixed for 5 min with Ponceau S stain (Sigma # P7170) and blocked for 1 h at 25 °C in 5% nonfat dry milk (wt/vol, BioRad #170-6404). Blots were probed with either C4F6 or SDG6 overnight at 4 °C followed by HRP-conjugated rabbit antibody to mouse IgG. Blots were visualized by chemiluminescence (Pierce #34095). Samples for denaturing western analyses were prepared in 4× loading buffer (Invitrogen #NP0007), separated by SDS-PAGE with 4–12% Bis-Tri gels (Invitrogen) in MES running buffer (Invitrogen #NP0002) and transferred to PVDF with transfer buffer (Invitrogen #NP0006-1). Unless otherwise noted, blots were processed as described above for native western blots.

Production of recombinant SOD1 proteins. To produce human wild-type SOD1 recombinant protein, the detailed protocol for insect cell expression and subsequent purification described previously was employed⁴⁹. The human wild-type SOD1 baculovirus stock was a generous gift from L. Hayward and A. Tiwari (University of Massachusetts Medical School). The established protocol was modified to use TN5B1-4 (High 5) cells from *Trichoplusia ni*, which were a generous gift from J. Francis and R.-J. Chain (Massachusetts General Hospital).

Recombinant SOD1ox was prepared by exposing human wild-type SOD1 to 10 mM H₂O₂ (Sigma)¹¹ at 25 °C for 16–24 h, after which the reaction was quenched by buffer exchanging SOD1ox into phosphate-buffered saline using a PD-10 column (GE Healthcare). SOD1 G93A was prepared as described above for wild-type SOD1. SOD1 H46R was a generous gift from L. Hayward and A. Tiwari (University of Massachusetts Medical School)⁴⁹. AS-SOD1 was a generous gift from J. Zitzewitz (University of Massachusetts Medical School)²⁶. AS-SOD1 was oxidized as described above for wild-type SOD1. Working aliquots of SOD1 were stored at –80 °C.

Epitope mapping analysis. GST-tagged SOD G93A full-length, and GST-tagged SOD G93A lacking one of the five exons were cloned into the pCDNA3.1 vector, and transfected into HEK-293T cells (American Type Culture Collection) with Lipofectamine 2000 (Invitrogen) according to manufacturer's instructions. Cells were then lysed with radio immunoprecipitation assay buffer (Boston BioProducts) supplemented with protease inhibitors (Roche, 11873580001). Extracts from cells expressing SOD1 G93C, G93D, G93R, G93S and G93V mutants⁸ were a generous gift from D. Borchelt and M. Prudencio (University of Florida).

Immunohistochemistry. Tissues were de-paraffinized through histology grade xylenes (three times for 5 min each) and a graded alcohol series (100%, 95% and 70% ethanol (vol/vol) twice for 2 min each). A method for antigen

retrieval (that is, acid, heat or proteolysis induced) was avoided when C4F6, the conformation-specific monoclonal antibody was used. Sections were incubated in 3% H₂O₂ diluted 1:10 in water from 30% H₂O₂ (wt/wt, Sigma), blocked with 10% normal goat serum (vol/vol, Jackson ImmunoResearch Laboratories) and incubated with C4F6 (1 μg ml⁻¹) prepared in antibody diluent (Dako, 3022) overnight at 4 °C. Sections were incubated with biotinylated secondary antibody to mouse followed by VECTASTAIN RTU ABC reagent according to the manufacturer's instructions (Vector Laboratories, PK-2200). Sections were colorimetrically developed using the 3,3'-diaminobenzidine substrate kit (SK-4100), and coverslipped with paramount.

For immunohistochemistry with the pan antibody to SOD1, the following procedure was used. Antigen retrieval was carried out with 0.01 mol L⁻¹ citrate buffer at pH 6.0 in an 800-W microwave oven for 10 min, twice, before immunostaining. The slides were stained on the DAKO Autostainer (DAKO). The sections were first blocked for endogenous protein binding and peroxidase activity with an application of Dual Endogenous Block (DAKO) for 10 min, and then with goat serum for 60 min. The sections were then incubated with a sheep polyclonal antibody (Calbiochem, 574597) at 1:100 overnight at 4 °C. Sections were then incubated with HRP-conjugated antibody to sheep IgG (Upstate, 12-342) at 1:500 for 60 min, and treated with diaminobenzidine for 5 min. The sections were counterstained with hematoxylin before sealing with permanent media.

Immunopurification and extraction wild-type SOD1 from human tissues. Individual immunopurification columns were prepared by coupling 3.5 mg of antibody to SOD1 (Binding Site, PC077) to 100 mg of cyanogen bromide-activated Sepharose 4B resin (Sigma, C9142) according to the manufacturer's instructions, and the antibody cross-linked resin was then transferred into Bio-Spin Columns (BioRad, 732-6008). Frozen SALS and control, lumbar or thoracic SpC tissue sections (~100 mg) were homogenized (Wheaton, 903475) in lysis buffer (25 mM Tris, pH 7.8, supplemented with protease inhibitors; Roche, 11873580001) at 4 °C and cleared by centrifugation at 18,000g and 4 °C. The pellet was stored at –80 °C, the cleared lysate was applied to an individual immunoaffinity column (1 unused column per sample) and the flow-through was saved on ice. The column was washed four times with 600 μl (~20 column volumes total) wash buffer (25 mM Tris, 100 mM NaCl, pH 7.8), followed by elution of wild-type SOD1 proteins with 2 × 500 μl of gentle antibody elution buffer, pH 6.6 (Pierce, 21027). The columns were re-equilibrated in lysis buffer, the flow-through re-applied, and the purification repeated for a total of 3 times to deplete the lysate of wild-type SOD1. Elutions were buffer exchanged into 25 mM HEPES, pH 7.4 using 10K MWCO Vivaspin concentrators (Sartorius, VS15RH01), and concentrated to ~100 μl with microcon concentrators (Millipore, 42406). The concentrations of wild-type SOD1 proteins were determined by western and densitometry (Image) analyses with recombinant wild-type SOD1 standards.

Wild-type SOD1 was extracted from the insoluble pellet using a modified protocol⁵⁰. Briefly, pellets were re-suspended in 1 mL washing buffer (50 mM Tris HCl, 100 mM NaCl (pH 7.4), 10% glycerol (vol/vol), 1% Triton X-100 (vol/vol), 0.5% NP-40 (vol/vol), protease inhibitor) and centrifuged (10 min) at 18,000g at 4 °C for a total of 4 times. The resulting pellet was re-suspended in re-solubilization buffer (50 mM Tris HCl, 100 mM NaCl (pH 7.4), 10% glycerol, 1% Triton X-100, 0.25 mM DTT, 1 mM EDTA, 2.5% SDS (wt/vol), protease inhibitor), heated to 100 °C for 20 min, sonicated (Transsonic 310) for 30 min, and heated again before centrifuging at 18,000g (10 min) at 25 °C. We subjected 5 μg total re-solubilized protein to a western analysis with an anti-SOD1 antibody (Calbiochem, #574597) as described above, except using the secondary anti-sheep IRDye800cw antibody (Rockland, 613-431-002), the Odyssey Infrared Imager (LiCor, Model 9120) and the Odyssey Software (LiCor, V3.0) for densitometry analysis. One μg total re-solubilized protein and 0.43 μg of the fourth wash that preceded the re-solubilization was visualized by silver stain analysis (Bio-Rad Laboratories' Silver Stain Plus kit, 161-0449) to check the total protein loaded to each well qualitatively.

The protocol above was used to extract SOD1 from fresh SpC tissue isolated from transgenic SOD1 G93A mice (B6/SJL, Jackson Laboratory) and naive mice (C57BL/6, Jackson Laboratory).

Vesicle motility assays in isolated squid axoplasm. Vesicle motility assays and immunoblot analysis of axoplasmic kinases were performed as described previously^{29,30}.



Mass spectrometry analysis of SOD1 proteins. Reversed-phase liquid chromatography was performed for wild-type SOD1 and SOD1ox (Fig. 1) using a two-dimensional nano-flow rate liquid chromatography (Eksigent), a 5-mm, 300- μm ID guard column (LC Packings, Part Number 160454) and a self-packed 14-cm, 100- μm ID column with 5- μm beads (taken from a larger Targa column). Buffer A consisted of 0.1% formic acid (vol/vol) in HPLC grade water and buffer B consisted of 100% HPLC-grade acetonitrile (vol/vol). Samples were diluted to a final formic concentration of 0.1% (v/v) and injected. Following injection, samples were washed on the guard column with 160 column volumes of buffer A ($8 \mu\text{l min}^{-1}$), and eluted at 650 nl min^{-1} using a 0–40% gradient over 30 min. For intact protein MS/MS, SOD1 was disulfide reduced in 50 mM tris(2-carboxyethyl)phosphine and 0.1 mM EDTA, desalted using C18 ZipTips (Millipore), and infused directly. Samples were introduced via a nanospray ion source with dual ion funnel (Apollo II) connected to a hybrid quadrupole Fourier transform ion cyclotron resonance (FT-ICR, FT-MS) mass spectrometer (apex Qe-94, Bruker Daltonics). The instrument was equipped with a hollow cathode for electron capture dissociation. External calibration of m/z scale was performed using electrospray tuning mix (Agilent, G2431A) using peaks at m/z 622, 922, 1522, and 2122.

After desolvation, the ions were transferred from a source hexapole to the quadrupole mass filter where isolation could occur in a second hexapole (collision cell). Ions accumulated in the second hexapole were then transferred through ion optics region of the instrument to the ICR cell. Frequency sweep excitation was followed by image charge detection. For the ECD experiment, activation of in the ICR cell was performed using a 105-Vpp, 1,000-Hz off-resonant, 4-ms sustained off-resonance irradiation during ECD pulse. Important instrument operation parameters include source declustering potential = 40 V, hexapole 1 accumulation time = 0.1 ms, collision cell accumulation time = 1 s, time of flight = 1.8 ms (D2), sidekick extraction voltages = -1.0 V (EV1, EV2, DEV2), RF excitation voltage = 130 V and ICR trapping

potential = 1.2 V; for MS/MS, Q1 m/z = 887.0 (for SOD1ox), isolation window (m/z) = 5, ECD bias = 6 V, ECD lens = 20 V and ECD duration = 4 ms.

Intact protein masses were reconstructed using the deconvolution function from DataAnalysis (Bruker Daltonics, version 3.4), and monoisotopic masses were determined using the Snap II algorithm (Bruker Daltonics). MS/MS data was automatically searched in human protein sequence database (MSDB) using Mascot TD and was matched to human SOD1 with trioxidation at Cys111.

For the analysis of AS-SOD1 proteins (Supplementary Fig. 1), samples were diluted in 0.1% trifluoroacetic acid (TFA, vol/vol) to $1 \mu\text{g } \mu\text{l}^{-1}$ and $5 \mu\text{l}$ was injected using a 10- μl loop injector onto a μ -precolumn C4 (Vydac) 15 mm \times 1 mm, 3 μm , 300 \AA (LC-Packings) using a flow rate of $50 \mu\text{l min}^{-1}$ with 10% acetonitrile and 0.1% formic acid. The mass spectra were acquired on a Q-Tof using W-mode (Waters) and the electro spray voltage set to 3,500 V. During the gradient, from 10% acetonitrile, 0.1% formic acid to 95% acetonitrile, 0.1% formic acid over 5 min, 3-s scans were collected from m/z 500–2,000. The spectra under the eluted peak were summed, and deconvoluted using MaxEnt1 (Waters).

Statistical analysis. A two-tailed Fisher exact test was used to determine the significance between SALS and control cases positively stained with the C4F6 antibody (Fig. 6). The activation of kinases in squid axoplasm and effects of FAT by SOD1ox (Fig. 5b) and insoluble levels of SOD1 in control and human tissues were tested using a pooled t test of $\mu 1$ - $\mu 2$ (Datadesk). $P < 0.05$ was considered to be statistically significant for all analyses.

49. Hayward, L.J. *et al.* Decreased metallation and activity in subsets of mutant superoxide dismutases associated with familial amyotrophic lateral sclerosis. *J. Biol. Chem.* **277**, 15923–15931 (2002).
50. Wang, L. *et al.* Wild-type SOD1 overexpression accelerates disease onset of a G85R SOD1 mouse. *Hum. Mol. Genet.* **18**, 1642–1651 (2009).